ELSEVIER

Contents lists available at ScienceDirect

Applied Thermal Engineering

journal homepage: www.elsevier.com/locate/apthermeng





Component-based modeling of ground-coupled seasonal thermal energy storages

Christoph Bott a,*, Mathias Ehrenwirth b, Christoph Trinkl b, Peter Bayer a

- a Department of Applied Geology, Institute of Geosciences and Geography, Martin Luther University Halle-Wittenberg, Von-Seckendorff-Platz 3, 06120 Halle, Germany
- ^b Institute of new Energy Systems, Ingolstadt University of Applied Sciences, Esplanade 10, 85049 Ingolstadt, Germany

ARTICLE INFO

Keywords:
Seasonal Storage
Thermal Energy Storage
Component-based Modeling
Matlab / Simulink
Large-scale TES
Planning and Design

ABSTRACT

Seasonal thermal energy storages are considered a central element of modern, innovative energy systems and help to harmonize fluctuating energy sources. Furthermore, they allow for an improved coupling between the electricity and heating sectors. Despite recent improvements of planning processes and enhanced models, significant discrepancies between projected and measured heat losses were revealed. Additional shortcomings of available tools relate to limitations in specifying geometry, internal design, or physical processes. Addressing these drawbacks, this study employs a revised, alternative approach by using a flexible, component-based, model ("STORE"). It allows variable flexible parameterizations to study diverse design scenarios. After introducing relevant seasonal thermal energy storage components, processes and mechanisms, datasets, and evaluation techniques, a plausibility test is presented that applies a common thermal energy storage model for benchmarking. In a test study, the re-use of a circa 1,000 m³ large swimming pool is simulated. STORE is used to investigate performance trends caused by different designs (e.g., insulation thicknesses, materials at individual interfaces). For the plausibility test, the results show a high degree of coverage and good applicability. Further, the results of the test study show a storage efficiency of 12.4% for an uninsulated base case, which can be improved to 69.5% in case of the most complex, highly insulated configuration. Critical trends are revealed, covering reduced peak capacity levels (26.5 to 23.5 MWh) and raised average filling temperatures (39.1 to 45.2 °C). Improved long-term behavior involves reduced environmental impacts due to reduced heating of the ambient soil (+7.9 K compared to +14.1 K after 2 years). General conclusions reveal that an optimal design should initially focus on an external cover of soil and top insulation. However, evaluations should base on multiple parameters depending on the target criteria. This is where the present model is highly useful. The capability of STORE to rapidly analyze a plethora of scenarios proves its high applicability for optimizing the planning processes of seasonal thermal energy storage projects.

1. Introduction

Today, around half of the global final energy consumption is related to the supply of heat used for industrial processes and domestic applications. Worldwide heat production relies heavily on fossil-based fuels and thus is carbon-intense. In contrast, non-biomass renewables contribute by a share of only 10–12% [1]. Due to their fluctuating nature, secure utilization of renewable sources such as solar thermal energy requires efficient temporal storage solutions, which in most cases

are realized as water-based sensible heat storage systems [2–5]. When applied to the seasonal storage of the solar energy abundant during the warmer months, these installations need to be sizable to minimize the relative heat loss until being used in the colder months.

There exist a variety of concepts ranging from domestic buffer tanks applied in residential buildings [6-10], via volume tanks or pools integrated into heating networks [11-15], to large-scale, earth-bound, openloop geothermal or closed-basin seasonal thermal energy storages (sTES). Geothermal implementations such as aquifer thermal energy storage (ATES) [16,17] and borehole thermal energy storage (BTES)

Abbreviations: ATES, Aquifer Thermal Energy Storage; BTES, Borehole Thermal Energy Storage; CFD, Computational Fluid Dynamics; FDM, Finite Difference Method; FEM, Finite Element Method; DHS, District Heating System; HDPE, High-Density Polyethylene; HX, Heat Exchanger; PE-X, Cross-Lined Polyethylene; RMSE, Root Mean Square Error; sTES, Seasonal Thermal Energy Storage; PTES, Pit Thermal Energy Storage; TTES, Tank Thermal Energy Storage; UA, Storage Thermal Envelope Value; WGTES, Water Gravel Thermal Energy Storage; XPS, Extruded Polystyrene.

E-mail address: Christoph.Bott@geo.uni-halle.de (C. Bott).

https://doi.org/10.1016/j.applthermaleng.2022.118810

Received 24 September 2021; Received in revised form 22 March 2022; Accepted 7 June 2022 Available online 10 June 2022

1359-4311/© 2022 The Authors. Published by Elsevier Ltd. This is an open access article under the CC BY-NC-ND license (http://creativecommons.org/licenses/by-nc-nd/4.0/).

^{*} Corresponding author.

Nomenclature		η	Efficiency (%)	
		o	Output vector	
\boldsymbol{A}	Interface or surface area (m ²)	p	Parameter vector	
α	Convective heat transfer coefficient (W m ⁻² K ⁻¹)	R^2	Coefficient of determination	
c	Specific heat capacity (J kg ⁻¹ K ⁻¹)	Re	Reynolds number	
d	Thickness (m)	ρ	Density (kg m $^{-3}$)	
D	Hydraulic diameter (m)	Pr	Prandtl number	
€	Surface roughness (mm)	Q'	Heat flow rate (W)	
h	Height (m)	Q	Energy quantity (MWh)	
i	Block input vector	s	State vector	
k	Radiation coefficient ()	t	Simulation time (s)	
λ	Effective thermal conductivity (W m ⁻¹ K ⁻¹)	T	Temperature (°C)	
ṁ	Mass flow rate (kg h^{-1})	ΔT	Temperature difference (K)	
n	Number of storage layers	V	Volume (m ³)	
Nu	Nusselt number		• •	

[18-22] strongly depend on site-specific (hydro-)geological conditions [23]. In comparison, closed solutions, such as tanks (TTES), pits (PTES) and water-gravel thermal energy storages (WGTES), represent artificial installations with engineered fillings, constructed walls, sealings and insulations [2,24–26]. These technologies are classified firstly according to their structural design. For example, PTES installations are naturally sloped excavations (e.g., former gravel pits), which are sealed with waterproofing membranes and usually comprise a floating top with integrated insulation. WGTES and TTES, in contrast, commonly include static elements such as vertical sidewalls, a foundation, and a selfsupporting roof. Aside from this, classification can focus on the filling of the storage: WGTES rely on a two-component filling media (matrix and fluid), while PTES and TTES are only filled with water [12,15,27,28]. Consequently, installations may also represent a combination of these storage types. The scope of this study is set on the category of artificial closed basins, which are less site-dependent than geothermal storage systems, but based on more complex engineered structures and devices.

Modern heating concepts do not only realize static seasonal storage but also flexible peak shaving and load shifting. Here, one seasonal cycle of solar supply is superimposed by secondary, short-term loads for integrating waste heat from industry, data centers, power-to-heat, or connected geothermal sources [29]. The design of the sTES may have a significant impact on the performance of the entire (district) heating system (DHS) [30]. Extended usability such as a storage device, buffer, and balancer, comes along with new performance requirements, which are ideally assessed and monitored by efficient computer-based simulations [19,31–33].

Available closed-basin sTES simulation techniques are manifold [34,35] and are performed most conveniently by assuming bulk efficiency coefficients or cycle losses [36-38]. However, this cannot resolve the transient thermodynamic behavior of storages, which is better tackled by process-based analytical [39] or numerical models, which often employ a finite element method (FEM) [40–42]. A comprehensive study on the state of the art of numerical modeling and simulation of sTES including a comparison of current tools is provided by Ochs et al. [43]. Accordingly, models for sTES analysis can be classified into five categories, ranging from energy system and building simulations (e.g., in TRNSYS [44,45] and Modelica [46,47] via computational fluid dynamics (CFD) and multiphysics approaches (e.g., in COMSOL [48] and ANSYS [49]) to subsurface modeling tools (e.g., FEFLOW [50]) [43]. These all differ in the level of detail, the scope of the components considered, and the spatial and temporal discretization methodology [25,51].

High-resolution CFD approaches were presented, for example, by Amiri et al. [52]. However, their model implemented in ANSYS-Fluent addressed turbulent airflow in small-scale packed beds of other use

cases and is not applicable to large-scale thermal storages. Among others, Bai et al. [27] and Fan et al. [53] found that detailed CFD models based on Navier-Stokes equations are only useful for detailed analyses of direct charging/discharging systems, as developed for instance by Sun et al. [54] or Powell et al. [55]. This is due to the generally high computational requirements of CFD simulation. The complex meshing has been identified as another drawback of CFD models [51,56]. A multiphysics FEM approach for detailed subsurface modeling has recently been demonstrated by Dahash et al. [51] using a model developed in COMSOL, whereby the radially symmetric configuration allowed for a reduction of computational effort.

A strongly simplified CFD setup focusing on thermal stratification was developed in Matlab by Bastida et al. [57] to analyze only the thermal behavior of the filling medium during direct charging/discharging processes within a cylindric, 100 m³ large TTES for different controller options. Within the Simulink environment, Ochs [58] developed a radially symmetric model, coupling a one-dimensional (1D) finite difference method (FDM) model for the storage filling (water) and a 2D-FEM model for the surrounding subsurface.

In TRNSYS, 3D approaches were developed as types 1300 (truncated cone, PTES) and 1301 (Surrounding Earth) for PTES [59]. The resolution of these models is limited to a 2D radially symmetric model of the subsurface and a 1D vertical setup of PTES. Type 1322, which is the latest but private development, merges these two domains for truncated pyramid geometries and enables a 3D resolution for the surrounding soil [60]. However, these models are also limited in the storage type and have a low resolution of the internal structure. Furthermore, material properties are only specified as constants and not all relevant processes are covered (e.g., solar irradiation). Different types for energy system simulation in TRNSYS model do not consider detailed internal storage processes at the component level, as the focus is on the performance within its connected energy system. A study by Li et al. [29] compared storage types 342, 343 and 534. Type 142/342 was developed to consider cylindrical water storage systems (TTES) as so-called "coarsestructure" [61] and was e.g., used by Sweet et al. [9] to determine optimal systems of individual houses with solar thermal energy. An alternative is type 343 ("ICEPIT") developed by Homberger [62], which offers modeling of alternative filling materials (e.g., gravel-water), yet it is limited to truncated cones. For geometry analysis, Bai et al. [27] applied coordinate transformation methods to a simplified sTES model (type UGSTS, [63]) in order to improve flexibility regarding slope angles and heights. However, the wall composites remained unresolved. A nonproprietary alternative is the tool developed and tested in a series of studies by Narula et al. [38,64,65]. It allows analyzing different configurations of energy systems, while the sTES sub-model is strongly simplified and lacks information about internal storage processes as well as environmental interactions. Before, Sorknæs [66] developed a

modeling tool optimized for an energy system consisting of solar thermal, heat pumps and a PTES and aimed at high computational speed, yet resulting in high errors (ca. 35%) of calculated heat losses. Within the Modelica/Dymola platform, Dahash et al. [67] and Reisenbichler et al. [68] developed models for simulating PTES to extend the Modelica Buildings Library [46,47] with large-scale applications. Again, these models are combinations of radially symmetric, 1D models for water fillings and 2D heat conduction models for PTES. They cannot resolve internal storage components and depict indirect charging/discharging methods, and they have limited flexibilities with respect to storage design and environmental conditions.

The objectives of this study are derived from the identified short-comings of existing applications. The aim is to provide a versatile model that captures relevant processes of large-scale, ground-based seasonal thermal energy storage basins, which can be adapted to any spatial scale, geometry, and time scale for fast system design, model-based control, and optimization. Furthermore, one goal is to implement processes, components, and system complexities that have not been sufficiently considered yet, with a particular focus on indirect charging/discharging systems. With the developed model, the simulation-based design process of a sTES is intended to be empowered by parallel, rapid and accurate analyses. On this basis, the aim is to enable straightforward parameter studies to rapidly identify the suitable configuration of a sTES system.

The novelties of the developed model relate to several aspects, while the modeling concept builds upon previous work and is intended to lend features from analytical and numerical procedures. For being straightforward to set up and use, as well as computationally efficient to execute, a component-based resolution of the storage device and ambient environment is employed. To ensure high flexibility, no limiting assumptions are made with respect to symmetry or radial configuration. This facilitates applicability to any geometry of the storage and resolves different lateral heat flux conditions in predefined discrete horizontal, and vertical directions. Thus, lateral, top, and bottom heat losses can be accounted for as well as effects of different insulation materials.

By discrete lateral process implementation, the geometric flexibility is maximized. Moreover, the model is able to cover complex designs (variable slope angles, height-dependent insulation thicknesses at different sides) or heterogeneous environmental conditions (e.g., heightdependent thermal conductivities). By achieving component-level detail, for example, unwanted, life-time-reducing temperature fluctuations in building components can be detected, while extensive parameterizations allow in-depth scenario analyses based on different material selections and thicknesses. This is not possible in models with compound U values or balanced UA values for larger domains. Additionally, one advantage is the consideration of energy gains and losses due to radiation to the ambient and solar irradiation to the storage's surface, as well as the ability to apply multiple temperature boundary conditions to different interfaces. Besides, detailed and flexible, indirect charging/ discharging mechanisms allow to evaluate temperatures, pressures, and energy fluxes. Implemented in Matlab/Simulink, the model allows flexible connectivity to other energy system components, while still providing a high resolution. It supports interfaces for further development, e.g., multiphysics co-simulations for implementing hydrogeological processes and/or soil heterogeneities, as proposed by Dahash et al. [56]. Ultimately, it is provided as a ready-to-use package with this study.

In the following, firstly, the new approach and its implementation ("STORE") is introduced. Second, a plausibility test is performed, which includes a benchmark against a commonly used and verified tool for simulation of hot water storages. Third, a test study with a total of 41 scenarios is defined. This is used to analyze the impact of variable storage configurations, ranging between a simple, uninsulated base case and a technically sophisticated high-tech case. The presented simulation results from these scenarios reveal storage performances, temperature

trends, and long-term environmental effects for different insulation thicknesses and materials. The findings enable the derivation of generalized design recommendations for storage projects of closed sTES facilities.

2. Materials and methods

2.1. STORE model

2.1.1. General approach

In contrast to highly resolving and computationally intense numerical sTES models, the present approach does not rely on a full, 3D spatial discretization of the simulated system. Instead, STORE distinguishes individual building components, resulting in a component-based approach similar to common "coarse models" [51,71,72]. The components are connected via process-based transfer functions, which control intercomponent exchange of thermal energy and thus determine the thermal regime for the given boundary and initial conditions.

Assuming a stratified storage model, vertical thermal interactions are only considered in the interior, i.e., the filling of the storage, which thus is resolved as 1D configuration. This also serves as a premise for related radially symmetric node models [9,25,39]. However, starting from this core, its shell is resolved to discrete directions (e.g. north, east, south, west, for representing a cuboidal geometry), including all building components as thermal masses. Between these, respective heat transfer processes are simulated, mostly conduction, but also convection and radiation. In addition, charging and discharging of the sTES facility is mapped in greater detail than by the addition or subtraction of energy quantities to/from thermal masses of the storage filling at defined heights. Existing analytical models and standard correlations of heat exchangers are used to include heat flows and processes of common components. Thus, other relevant mechanisms of the charging and discharging processes, such as pipe hydraulics, are considered. The concept offers the advantage of being able to investigate variable geometries (e. g., multi-basin storages) and technically sophisticated configurations with a flexible choice of building materials and methods.

STORE is developed in the Matlab/Simulink environment [73]. The underlying concept in Simulink is commonly known as bond graph modeling. Here, the model is based on function blocks containing input (i), output (o) and state (s) vectors, together with associated parameters (p). During simulation, states can be represented in discrete-time (s_c) or continuous-time (s_{d_k}) form, following the mathematical relationships for outputs (eq. (1)), derivatives (eq. (2)), and time-stepping updates (eq. (3)):

$$o = f_0(t, s, i, p) \tag{1}$$

$$\dot{s}_c = f_d(t, s, i, p) \tag{2}$$

$$s_{d_{k+1}} = f_i(t, s, i, p) \tag{3}$$

Moreover, Simscape [74] is used as a supplementary toolbox to build a physical model with preexisting subfunctions. Within its open-source foundation library, underlying equations of all processes are accessible. The distinctive feature of Simscape is the ability to allow bidirectional flows between function blocks, in order to allow component-based, physical modeling. Thus, all components are configured as a block diagram including the specification of coefficients and variables, for example, material thicknesses, surface areas, and heat transfer coefficients in case of heat conduction. The simulation procedure involves the initialization of the model, where block parameters and the initial conditions are set. Numerical integration is performed in STORE using the ordinary differential equation solver ode23t, which solves initial state equations and runs the simulation using the FDM discretization method. The maximum step size is set 3,600 s, to calculate accurate results on an hourly basis. Consistency tolerances for initial conditions and transient calculation are set 10⁻⁹ to provide a reasonable

trade-off between computational accuracy and simulation time. Using Matlab/Simulink offers further advantages: First, pre- and post-processing procedures can be incorporated in transparent fashion, for example, to read load profiles or to perform any follow-up evaluations, such as the determination of efficiency indicators. Second, a design database can be generated in advance, providing a simple way to perform parametric or sensitivity studies. For this, different scenario specifications can be run in parallel, ensuring optimal utilization of computational resources.

For parametrization, the design scenario database represents a further, novel key aspect. It contains all material properties of all individual domains, information about the basin's geometry, as well as other relevant parameters for design and operation. The structure and contents of the database are illustrated in Supplement 1.

2.1.2. Modeled components and processes

Fig. 1 shows the structure of a storage system and its implementation in the component-based STORE model. Here, the cross-sectional view of Fig. 1a illustrates the individual components of the storage shell, which are resolved as thermal masses. By default, the components involved, from the interior to the exterior are: (i) the filling medium, (ii) an internal sealing, (iii) the insulation material, (iv) an external sealing, (v) the structural component (i.e., sidewall), and (vi) multiple thermal masses for providing a transition to the surrounding soil. Internal and external sealing layers are required for storage systems, where the bulk insulation material is placed between two waterproofing membranes, as is common practice [2,75,76]. In the technical implementation of the model, thermal masses and transfer functions are grouped into assemblies. This allows flexible adaptation to different concepts or designs, which may also cover composites of multiple, partitioned basins with intermediate walls, which cannot similarly be considered with symmetric sTES models. Likewise, parallel or serially combined setups can be simulated.

As a stratified sTES model, STORE is divided into n vertical sections using a height fraction (h_{layer}) based on the height of the storage filling (h_{sTES}) according to:

$$h_{layer} = \frac{h_{sTES}}{n} \leftrightarrow h_{sTES} = n \cdot h_{layer} \tag{4}$$

This ensures that the internal storage height is uniformly divided and that the thermal masses represent the corresponding fractions of the building. The absolute elevation of each layer, i.e., its position within the storage, is used to automatically assign height-dependent parameters (e.g., fill volumes due to lateral slope angles, decreasing insulation thicknesses towards the bottom of the storage, etc.). The geometric flexibility of the model is exemplified in the cross-sectional view in Fig. 1a as a variable insulation thickness at the top and the bottom as well as height-dependent at the sidewalls. This exemplary setup represents a configuration with ten vertically arranged layers, whereby the thermophysical, vertical interconnections between the thermal masses

of the filling and the top and bottom assemblies are depicted. The laterally modeled processes are indicated in the central layer. However, this view shows that gaps are left in the model corners, where the discrete, spatial directions diverge. For simplification, influences between the different directions are neglected here. Instead, adiabatic boundary conditions are assumed. The top perspective in Fig. 1b illustrates the lateral arrangement of the components in one horizontal layer, while the structure in this configuration is based on a rectangular base plane. However, the model allows other shapes and even a cylindrical design to be realized by a straightforward reconfiguration approach. Contrary to many other models used for sTES [27,31,53,57], here, the model's structure is not radially symmetric.

The superordinate, simplified energy balance of the sTES under consideration (eq. (5)) consists of the energy stored in the storage's filling Q_{sTES} , the charging/discharging fluxes (Q_{ch} , Q_{dis}), and interactions with the ambient ($Q_{sol,out}$ radiation to the ambient, $Q_{sol,in}$ for solar irradiation, Q_{soil} and Q_{air} for energy exchange with the surrounding soil/air), based on the thermal transfer functions described below:

$$Q_{sTES} = \dot{Q}_{ch} + \dot{Q}_{sol,in} - \dot{Q}_{dis} - \dot{Q}_{sol,out} - \dot{Q}_{soil} - \dot{Q}_{air}, \text{ where } Q_{sTES}$$

$$= c_{fill} \cdot V_{fill} \cdot \Delta T_{sTES}$$
(5)

Besides, the energy balances of the individual components are defined based on all processes at their respective positions. For example, exchanges of energy by radiation $(\dot{Q}_{sol,in}, \dot{Q}_{sol,out})$ are associated only with the thermal masses of the uppermost layer. Thus, the energy balance of these thermal masses changes accordingly. Heat transfer between all components is quantified by several thermal transfer functions, as illustrated by the arrows in Fig. 1. Here, vertical connections only exist between the thermal masses of the filling, and in the top and bottom sections, where thermal interactions with the ambient air or soil occur.

As a prevailing process, thermal conduction, which depends on the provided material parameters (effective thermal conductivity λ_{eff} , thickness d, interface area A), is simulated laterally on each layer and in the vertical direction between the thermal masses of the filling. The governing equation used is Fourier's law, described as:

$$\dot{q}_{cond} = \lambda_{eff} \frac{A}{d} \Delta T \tag{6}$$

In the storage's filling, however, thermal conduction only dominates for indirectly charged and discharged water-gravel storages, where flow paths are assumed to be strongly limited. Thus, buoyancy effects are neglected in the current version of STORE. In contrast, for pure water fillings (e.g., in the case of TTES systems), and to model subordinated mixing effects due to convection in WGTES during longer standby periods, convection can be included as an essential process using the corresponding parameters (convective heat transfer coefficient α , interface area A). Heat transfer by means of convection is modeled using Newton's law of cooling:

$$\dot{q}_{conv} = \alpha \cdot A \cdot \Delta T \tag{7}$$

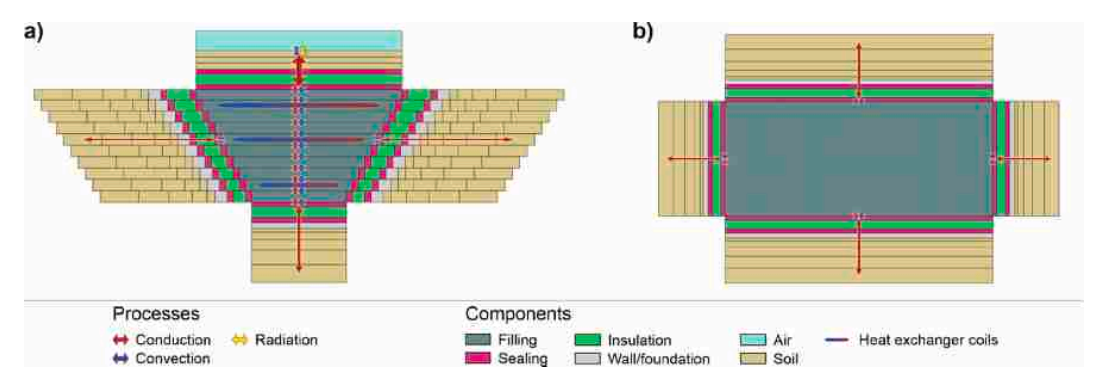


Fig. 1. Conceptual design of the model with components in cross-sectional view (a) and top view (b).

By default, the top part of the STORE model reflects the sidewall configuration, including internal and external sealings with an interposed insulation. A static component is included, e.g., for water-filled tanks with self-supporting roofs. Furthermore, a key component represents an external top covering of the storage (e.g., soil), which is particularly relevant for low-insulated systems. To take higher thicknesses of the top covering and a steeper temperature gradient to the air into account, this component is resolved by three thermal masses. Radiation is also introduced here as a further thermal process using the equation of Stefan-Boltzmann, based on the radiation coefficient k, the emitting surface area A, the distance, and the temperatures of two thermal masses T_A and T_B [77]:

$$\dot{q}_{rad} = k \cdot A \cdot \left(T_A^4 - T_B^4 \right) \tag{8}$$

As the considered sTES technology types are in-ground structures, the same configuration as the lateral storage shell is realized in the bottom part of the model. However, instead of the sidewall, conduction through the storage's foundation and transition to the underlying soil are modeled.

STORE is primarily used to model WGTES systems, which employ indirect heat transfer via an internal coil system as a heat exchanger (HX) for charging and discharging on multiple, predefined levels [2,78,79]. Hence, no operation involving fluid mass transfers at inlets and outlets of the filling is considered and mass conservation is ensured anytime. The number of charging/discharging levels as well as their absolute height in the filling are governed by the model's structure (Fig. 1a). The coils of the HX are mapped using a pipe flow model obtained from the Simscape library, allowing fluid flow to be described analytically. Based on mass flow rates and temperatures of the charging fluid, as well as geometrical and material specifications, conductive and convective heat transfer (to obtain the values of Q_{ch} , Q_{dis} of the system's energy conservation equation), and pressure loss by friction at the pipe walls, are simulated. Heat transfer at the pipe wall due to conduction is calculated based on the hydraulic diameter of the pipe (D), the thermal conductivity of the charging/discharging fluid (λ_l), the surface area of the pipe wall (A_P) , the pipe wall temperature (T_P) and the charging/ discharging fluid's temperature at each pipe node (T_{In}):

$$\dot{q}_{PipeCond} = \left(\frac{\lambda_l \cdot A_P}{D}\right) \cdot (T_P - T_{ln}) \tag{9}$$

Eq. (10) is used to calculate heat transfer due to convection, based on the fluid's average specific heat $(c_{P,Avg})$, its average mass flow rate through the pipe (m_{Avg}) , its temperature at the inlet (T_{In}) , its average thermal conductivity (k_{Avg}) , the Nusselt number (Nu) and the hydraulic diameter (D).

$$\dot{q}_{PipeConv} = c_{p,Avg} \cdot \left| \dot{m}_{Avg} \right| \cdot (T_P - T_{In})$$

$$\left[1 - \exp\left(\frac{Nu \cdot \lambda_{Avg}}{D} \cdot S_H \right) \right]$$

$$c_{p,Avg} \cdot \left| \dot{m}_{Avg} \right|$$

$$(10)$$

Turbulent flow is modeled analytically via the Gnielinski correlation [80–82], using the Nusselt number (Nu) as a function of Reynolds (Re) and Prandtl numbers (Pr), the hydraulic diameter (D) and the internal surface absolute roughness (ε_R):

$$Nu = \frac{\frac{f}{8} (Re - 1000) \cdot Pr}{1 + 12.7 \cdot \left(\frac{f}{8}\right)^{\frac{1}{2}} \cdot \left(Pr^{\frac{2}{3}} - 1\right)}$$
with $f = \left\{ -1.8 \log_{10} \cdot \left[\frac{6.9}{Re} + \left(\frac{\epsilon_R}{3.7 \cdot D}\right)^{1.11}\right] \right\}^{-2}$

To analyze the behavior of the charging/discharging system and temperature fluctuations which may cause adverse effects on the materials used, conductive heat transfer through the pipe walls is coupled to the pipe model prior to heat transfer to the filling. A graphical representation of the developed model showing boundary conditions, fundamental equations of modeled processes, and initial conditions is also available in Supplement 2.

2.1.3. Boundary conditions of environment and storage operation

Lateral energy exchange with the ambient ground is simulated in each layer as conduction through the surrounding soil at a resolution of five serially arranged thermal masses. In order to ensure a sufficient distance between the outer wall of the storage and the boundary of the model, their distances (i.e. volumes or thermal masses) can be adjusted and assigned with a linear increment. Preliminary studies during model development showed a required minimum distance of 2 m and a recommended increment of 2 m. However, these values may be modified for specific studies, depending on dimensions and operating conditions of the facility, while probe points may be used to verify sufficient distance. At the end of this sequence, interference with the ambient ground is modeled by a transient, specified temperature boundary condition $(T = T_t)$, based on an annual temperature profile T_t . This temperature can further be specified as a depth-dependent variable, which can be a decisive characteristic for the considered, buried, artificial basin structures. At the top, interactions with the unsaturated zone occur, while at the bottom, interactions with the groundwater may exist. Ambient groundwater flow cannot directly be simulated in STORE, but increased effective thermal conductivities of the soil due to groundwater flow may be used as a proxy to account for higher energy losses by heat dissipation.

The top part of STORE contains a component of surrounding air, where losses by convection and radiation are simulated. Similarly, an annual air temperature profile is laterally coupled to this component by a transient, specified temperature boundary condition. Energy gains by solar irradiation are modeled by a transient, specified heat flow rate boundary condition, which uses an irradiation profile (P_t) directly linked to the external top covering (surface area A_{Top}):

$$\dot{q}_{sol,in} = \frac{P_t}{A_{Ton}} \tag{12}$$

Hence, required weather data may be obtained from nearby stations and contain temperature time series for air and soil, while groundwater temperatures replace soil temperatures in the lower sections in case of high groundwater levels, or if soil temperature data is not available.

The connected DHS is represented by a boundary condition based on load profiles, which covers temperatures and volume or mass flows. Time-resolved datasets provide information on supplied charging energy or demands for discharging and are directly linked to the analytical HX model (eqs. 9–11). However, the presented model aims at longer-term operation over several months and years and prefers hourly resolved datasets. Since the DHS is not modeled explicitly, feedback effects caused by temperature alterations of the storage cannot be quantified.

To simulate the system's operation, a control function is defined, governing charging and discharging operations, as well as idle phases. To illustrate a default operation strategy, Fig. 2shows a flowchart of operation mode decisions.

There, decisions are based on the storage's state (i.e., filling temperature, $T_{Storage}$) and on the availability of charging supplies or discharging demands respectively, while a superordinate check uses maximum or minimum thresholds (T_{max} , T_{min}) to protect components by not exposing them to excessively high or low temperatures. The return temperature of the heat exchanger (T_{Return}) is used to reflect the available energy flow for discharging. Time and temperature hystereses may optionally be included, to allow sufficient time for slow processes of heat propagation within the storage and to prevent rapid changes in operating modes, thus preventing stress on building components and pumps.

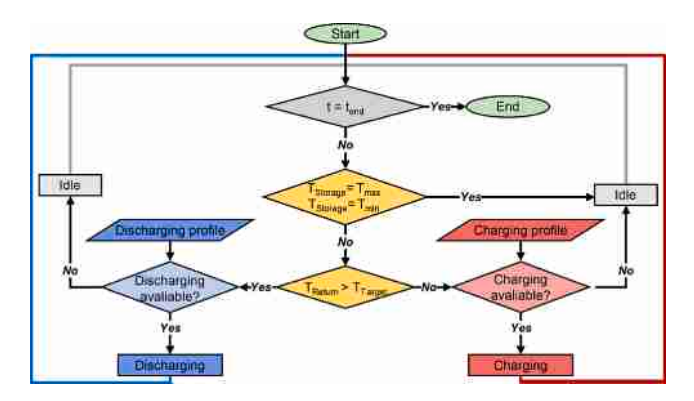


Fig. 2. Simplified flow chart for sTES control: Hystereses or subordinated strategies, e.g. with transition periods, are not considered. t: simulation time, $t_{\rm end}$: last simulation time step, $T_{\rm Storage}$: temperature reference of the storage, $T_{\rm Target}$: temperature of the target system.

2.1.4. Outputs and efficiency evaluation

STORE is equipped with an extensive configuration of default probes for monitoring (default configuration explained in Supplement 3). These analyze information on operation states, temperatures and energy flows in the storage, the HX, as well as interactions with the ambient, or any other physical measures. Thus, a variety of outputs are generated for evaluating the storage's behavior and performance in different scenarios.

For endpoint evaluation, temperatures and energy flows represent initial rating metric. Furthermore, the efficiency is calculated based on two different approaches. Regarding the connected DHS, the amount of energy supplied by the storage via discharging is determined:

$$\eta_{\textit{Subsystem}} = \frac{\sum Q_{\textit{Discharged}}}{\sum Q_{\textit{Charged}}} \tag{13}$$

Accordingly, this subsystem efficiency, $\eta_{Subsystem}$, is obtained from the ratio of discharged and charged energy quantities, both given in MWh, specified over a defined period. This indicator is particularly important for evaluating the potential for energy conservation, as the utilization of energy from the sTES may substitute other sources, which could emit greenhouse gases or be costlier. Thus, it is a practice-oriented parameter, which is focused on the benefits of a given storage facility. In contrast, the accumulated surpluses in the sTES are also of particular interest in multi-year storage operation or in case of a temporal or quantitative imbalance between demand and supply of thermal energy. Therefore, the system-related efficiency is compared to an internal storage efficiency, $\eta_{Storage}$, which is used to evaluate the raw efficiency of the sTES building to store thermal energy at low losses.

Accordingly, it is defined as the ratio of total energy losses to the total quantity of energy stored over a specific period and considers remaining excess energy quantities at the end of the observation period:

$$\eta_{Storage} = 1 - \frac{\sum Q_{Loss}}{\sum Q_{Charged} + Q_{Excess}}$$
 (14)

A clear distinction between these two endpoint parameters is evident in the application case, as well as in the scope of balancing. This is critical, as the consideration of excess energy contents at the end of an observation period may significantly affect the storage's performance. Likewise, in the heat-up phase of a sTES, these values are strongly deviating, given the high imbalance between the storage and its environment. In this case, an evaluation regarding the energy quantity dissipated to the environment is of higher interest and should be separated from the direct discharge evaluation.

The operation time is discretized by given time frames and all values are expressed in MWh. For seasonal storage, consecutive cycles (mostly on the annual scale) are most appropriate. Initial heating phases deserve special attention, which often are most dynamic before the facilities

converge to a quasi-stationary state. Therefore, the period until this state is reached serves as a further decisive performance criterion.

2.2. Plausibility test

To determine the accuracy of the newly developed model, a plausibility test is first performed comparing STORE to a homogeneous body without thermal stratification. Thermal losses across the shell are distinguished from surfaces with contact to the air (top) and the surrounding soil (bottom and sides). The ambient temperatures are linked to these surfaces without interposed components, while the shell is described as a single component with a balanced value for thermal conductivity of the total compound, preventing resolution at the component level. Charging and discharging mechanisms are implemented using a simplified heat exchanger equation with homogeneous heat transfer to the entire body. With this simplified model, a basic energy balance is solved, calculating storage energy contents and temperatures based on charging/discharging energies, as well as interactions with the environment.

In a second step, results of a benchmark scenario are compared to an experimentally verified model. A customizable thermal storage model of the CARNOT toolbox (Storage Type 3) is used in this instance [70,83]. It bases on a similar approach of Type 342 of TRNSYS, using a 1D node model [9,61]. In comparison to the presented component-based model, it supports only one temperature boundary condition and the storage shell is represented as a compound structure. Furthermore, it relies on a radially symmetric setup, and thus only cylindrical geometries with uniform sidewall configurations can be modeled.

Therefore, in contrast to the configuration shown in Fig. 1, the geometry of STORE has to be simplified for comparability to a rectangular $20~\text{m} \times 20~\text{m} \times 10~\text{m}$ (length, width, height) basin. A best-fit geometry with equivalent UA values is calculated for the parametrization of the CARNOT model, assuming similar external surface areas at minimal differences in diameter and height. To closely approximate the charging and discharging processes, modifications additionally involve replacing the default heat exchanger in the Storage Type 3 model with a pipe model with similar specifications. The test covers a facility completely surrounded by soil. The influence of the surroundings is minimized using small volumes for the surrounding soil thermal masses in STORE. Further a homogeneous insulation at all sides with a thickness of d = 0.3m and a thermal conductivity of $\lambda = 0.1~W~m^{-1}~K^{-1}$ is assumed. With these settings, different simulations of storage operation were performed. As an example, the presented results in section 3.1 cover a cooling curve starting from a filling temperature of 75 °C with static ambient conditions (20 °C).

2.3. Test study scenarios

To further evaluate the capabilities of STORE, a test study with a variety of scenarios is conducted. A typical application of the model is used where a robust feasibility assessment of an existing installation is needed in the design process. Here, STORE perfectly meets challenging demands of flexible parameterization to evaluate a large number of scenarios in order to provide design recommendations for an optimal solution.

Assuming generic load profiles and environmental characteristics, five years of operation are simulated. Different material parameters, conceptual and geometric settings of sTES are varied to identify crucial aspects for system optimization. An overview of the simulated scenarios is provided in Table 1. An uninsulated storage serves as the base case, which is modified in subsequent steps, assuming different external top covers, insulation thicknesses, and materials at the different sTES interfaces. By separately considering these aspects, efficacies of the various optimizations are to be determined. The results are evaluated with respect to the measures of efficiency (eqs. (13) and (14)) and storage temperature characteristics, both covering the entire operation

Table 1Variables and parameters used for the test scenarios. XPS: Extruded polystyrene. HX: heat exchanger.

Domain	Parameter	Top covering (m), increment	Insulation thickness (m), increment: 0.05			No. of scenarios
			Тор	Sidewalls	Bottom	
Base case	Uninsulated storage system - HX spacing: 1.00 m - HX diameter 0.05 m	0		0		1
Top covering	→ Thickness (m)	0.251.00,		0		4
		0.25				
Insulation thickness	▲ Top (Foam glass)	0	0.050.3	0	0	6
	Sidewalls (Foam glass)	0	0	0.050.3	0	6
	▲Bottom (Foam glass)	0	0	0	0.050.3	6
Insulation material		0		0.050.3		6
	-O-Top, sidewalls: XPS	0		0.050.3		6
	Bottom: Foam glass					
	Top: Mineral wool	0		0.050.3		6
	Sidewalls, bottom: Foam glass					
Total number of scenario						41

period and the last simulated year.

2.3.1. Setup of the seasonal thermal energy storage facility

Fig. 3shows the conceptual outline and geometry of the basin structure for all scenarios of the test study. It has a cuboid shape with internal dimensions of $25 \times 12.5 \times 3.0$ m, which is completely embedded in surrounding subsoil. These are chosen based on the approach of the re-use of existing infrastructure (here: swimming pool) for seasonal thermal energy storage. Previous studies [12] already discussed such a scenario, for example, to optimize heat pump operations by using an outdoor pool as a seasonal source of heat and cold [84,85]. With a surface/volume ratio of 0.90 m $^{-1}$ this case is suboptimal in comparison to other storage basin geometries and considering the optimum ratio of 0.49 m $^{-1}$ for a sphere with the same volume. However, for such unfavorable conditions, understanding and managing lateral heat loss is particularly of high importance.

The storage media is a water-filled gravel matrix with a grain size between 16 and 32 mm. Based on existing field cases [78,79], a porosity of 0.4 is assumed, resulting in a total specific heat capacity $c=1,545~\mathrm{J}$ kg $^{-1}~\mathrm{K}^{-1}$ for the composite filling material. Effective thermal conductivity is set $\lambda_{eff}=2.4~\mathrm{W}~\mathrm{m}^{-1}~\mathrm{K}^{-1}$ according to measured values of the WGTES facilities in Chemnitz (Germany) and Steinfurt-Borghorst

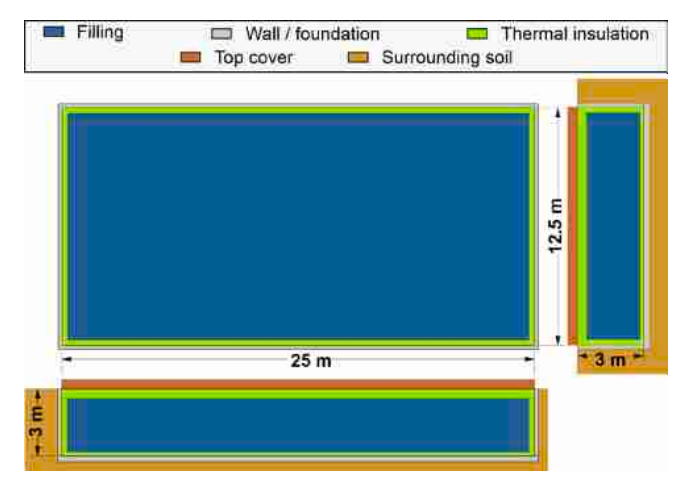


Fig. 3. Top and side views of the sTES structure of the test study, with an illustration of filling, thermal insulation, walls and foundation, as well as external top covering and surrounding soil (suppressed in the top view).

(Germany) [75,86,87]. Convective heat processes are assumed to be minimal, quantified by a convective heat transfer coefficient in the filling of $\alpha = 0.1$ W m⁻² K⁻¹. In the sTES, rigid cross-linked polyethylene (PE-X) pipe coils are installed as a heat exchanger. The internal spacings of the installation grid as well as the distances to the sidewalls of the basin are kept constant at 0.1 m. The pipe wall thickness is assumed to be 5 mm. The heat exchanger is installed at three levels within the storage filling, at 25%, 50%, and 80% of the total filling height.

A supporting shell structure of concrete is built up by vertical sidewalls with a constant thickness of 0.2 m and a foundation of 0.3 m. The sealing layer consists of two 2 mm thick high-density polyethylene (HDPE) foils. In the scenarios focusing on variable thermal insulation of the system, the insulation layer is embedded between these foils. It is important to note that, for similar temperatures, increasing insulation thickness reduces the filling's volume and thus the capacity of the storage. Foam glass gravel is among the most commonly used materials [2,5,25] and thus selected as the default insulation material. It is characterized by a low thermal conductivity of $\lambda = 0.05 \text{ W m}^{-1} \text{ K}^{-1}$ and a low density of $\rho = 160 \text{ kg m}^{-3}$ [88,89]. Moreover, it is anti-capillary as well as pressure-resistant, which is particularly relevant because of higher loads at the bottom in the case of gravel-water fillings [88]. In comparison, XPS and mineral wool represent more cost-effective materials with better thermal properties ($\lambda = 0.04 \text{ W m}^{-1} \text{ K}^{-1}$ for XPS and $0.03 \text{ W m}^{-1} \text{ K}^{-1}$ for mineral wool, [90]). However, since they are not pressure-resistant, they are applicable only at the top and sidewalls. These alternatives are investigated in twelve different "insulation material scenarios" (Tab. 1).

In order to compare the base case of a simple setup (without internal thermal insulation and external top covering) to a technically sophisticated variant, a high-tech case is defined. In this scenario, the basin is equipped with the most thermally effective insulation components, and at the same time, it represents the potentially most expensive design option. Each of the three interfaces of the storage filling is equipped separately: while the top is equipped with a 0.3 m thick layer of mineral wool, the sidewalls are insulated using 0.3 m XPS layers. At the bottom, foam glass gravel with a thickness of 0.3 m is applied. Due to the substantial use of insulation material, the storage volume is reduced in this high-tech scenario from 937.5 m 3 to 696.9 m 3 , while higher temperatures may counterbalance this reduction of the static capacity.

2.3.2. Boundary and initial conditions

For simulation of the storage operation, synthetic load profiles of a connected energy system are applied. As realized in practice [41,79,91], it is assumed that the facility is integrated into a decentralized solar

thermal system with a small-scale DHS, while the modeled sTES is assumed to be hydraulically decoupled from the connected DHS. With one operating cycle per year, the scenarios represent seasonal charging/discharging. Thus, energy losses of infrastructures beyond the simulated storage as well as efficiencies of heat exchangers are neglected.

The annual charging load profile is shown in Fig. 4 (red), comprising a constant volume flow rate of 10 m 3 h $^{-1}$ and a constant HX inlet/supply temperature level of 50 °C in summer. Since the storage is only used for heating of residential buildings in winter, the opposite period used for discharging is shown in Fig. 4 in blue, with a constant HX inlet/supply temperature of 15 °C and a volumetric flow rate of 20 m 3 h $^{-1}$. Temperature and temporal hystereses are set to 5 K and 12 h.

In this test study, environmental conditions during storage operation depict the city of Ingolstadt, Germany. To specify the boundary conditions, the German Weather Service (Deutscher Wetterdienst, DWD), in cooperation with the Federal Institute for Research on Building, Urban Affairs and Spatial Development (Bundesinstitut für Bau-, Stadt- und Raumforschung), provides datasets on test reference years [92]. These are commonly used for the simulation of energy systems in construction projects. Hourly resolved air temperatures and solar irradiation datasets were obtained for moderate weather conditions throughout a reference period from the year 1995 to 2012 (Fig. 5). For specifying the thermal conditions in the embedding soil, local, long-term measurement series of soil temperatures at a depth of 1 m from a nearby weather station result in an average annual temperature profile, shown in green in Fig. 5b. Any influence of ambient groundwater flow is neglected.

The material properties of the surrounding soil and the external top covering are oriented at standard values for dry soil ($\lambda=2.2~{\rm W~m^{-1}~K^{-1}}$, $c=800~{\rm J~kg^{-1}~K^{-1}}$, $\rho=1,500~{\rm kg~m^{-3}~[90]}$; k=0.95~[93]). In contrast to the internal insulation components, the top covering is applied externally and does not reduce the volume of the storage's filling. The thickness of the five surrounding soil blocks starts at 2 m and further increases linearly at increments of 2 m, in order to facilitate sufficient distance from the storage's external walls and to prevent interfering influences of boundaries.

It is assumed that between completed construction and commissioning of the facility, the basin is at thermal equilibrium with its environment. Therefore, all thermal masses, both inside the investigated sTES (i.e., fillings, insulation, seals, static elements) and outside (top covering, surrounding ground) are initialized with the soil temperature at the moment of commissioning (assumption: beginning of a fiscal year, 1st of January, 4.43 $^{\circ}$ C). The charging/discharging system is initialized unpressurized (not operating) without initial mass flow in the heat exchanger coils.

3. Results and discussion

3.1. Results of plausibility test

The results of the plausibility test are shown in Fig. 4 and include the

individual temperature profiles of the cooldown curves (average, minimum and maximum temperatures of the sTES layers) simulated with the model of the CARNOT toolbox and the newly developed STORE model (Fig. 6a). Furthermore, Fig. 6b depicts the differences between CARNOT and STORE, which reach 0.93 K and -1.21 K (RMSE max. 0.396 K), while both models correlate by at least $\mbox{R}^2=0.947.$

The remaining discrepancies are explained by the conceptual differences of the two models, which also evolve because no additional adjustment procedures (e.g., further refinements of UA values) were considered. While the CARNOT toolbox applies a radially symmetric 1Dnode model [83], the presented component-based approach of STORE is optimized for rectangular configurations. Additionally, more flexible temperature boundary conditions for modeling environmental conditions are used, including different temperatures at exterior interfaces and multiple thermal masses of soil embedding the storage basin. In this way, the outwardly decreasing temperature gradient is simulated and the additionally activated thermal capacity of the surrounding soil is considered. In the results of the simulation, these design disparities are reflected as trailing effects: initially, the temperature differences between the two models show a negative tendency (i.e., adverse effects), but then develop slightly higher values (i.e., positive effects). Having these conceptual differences in mind, the model comparison is considered successful, indicating a robust applicability of the model. Furthercomparison method, including parameterization script for the CARNOT model, may be included as a subcomponent within the model, in case further analyses are desired. This option allows for parallel benchmark comparisons for subsequent studies.

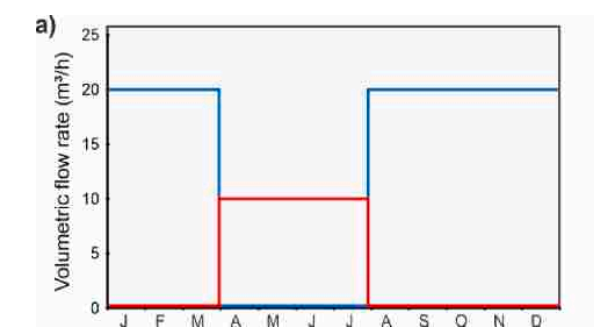
3.2. Evaluation of the test study

3.2.1. Base case vs. High tech case

The results of the test study start with the most simple and non-insulated base case (Fig. 7a-d) in contrast to the technically most complex high-tech case (Fig. 7e-h) and the results for the described seasonal 5-year operation of the storage are presented. The recorded energy quantities of charging, discharging and losses, temperature key parameters, capacity levels of the storage facility, as well as efficiency endpoint parameters are examined.

The base case system performs quite poorly, as the subsystem efficiency only reaches 11.6% in the last simulated year. Peak capacity levels of the uninsulated basin reach 26.5 MWh (Fig. 8a), with a fraction of 59.8 MWh recovered (i.e., discharged) of the 444.8 MWh charged energy over the five simulated years. The heat losses and interactions with the environment are highest in this scenario, with an average of 91.6 MWh per year. This leads to a derived storage efficiency of 12.4%. The maximum and average storage temperatures over the entire simulation period are 42.8 °C and 39.1 °C, respectively (Fig. 8b-c).

Evaluations of the high-tech scenario reveal a much higher storage efficiency of 57.1% and a subsystem efficiency of 69.5%. However, due



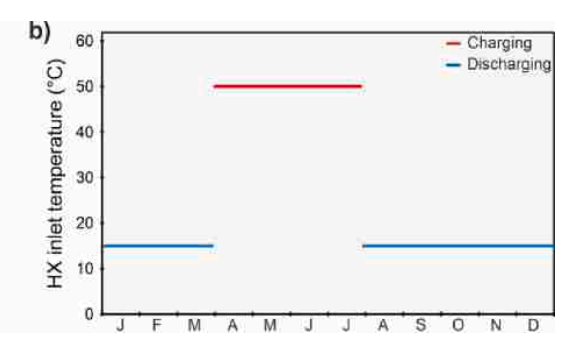
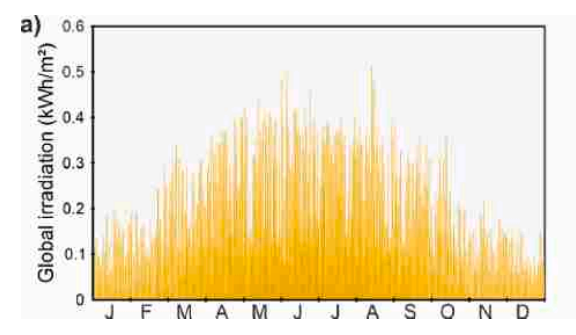


Fig. 4. Illustration of the annual load profiles for charging and discharging with a) volumetric flow rates and b) inlet/supply temperatures of the heat exchanger (HX).



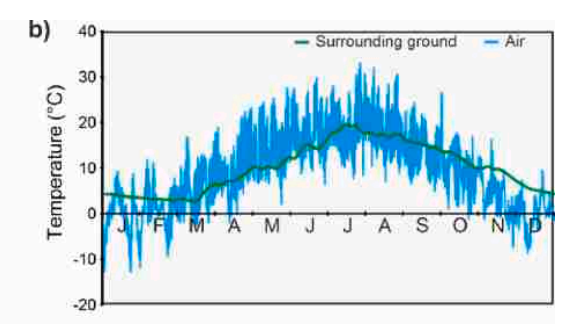


Fig. 5. a) Annual temperature profile of potential energy gain through hourly global irradiation from the sun as well as the b) hourly resolved annual temperature profile of ground and air temperature.

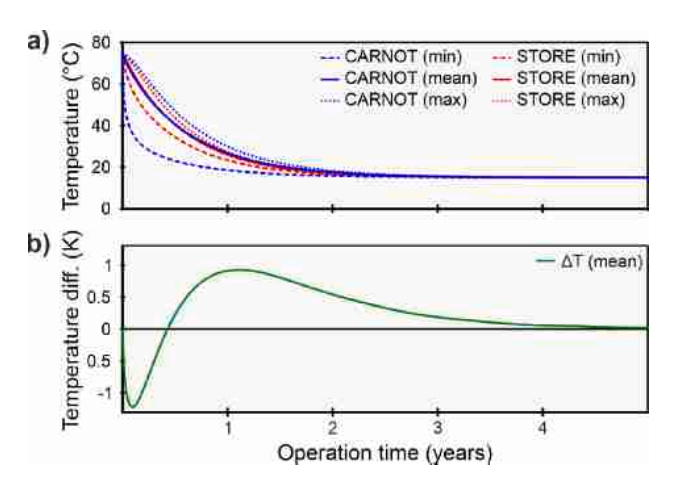


Fig. 6. a) Cooling curves of the STORE model and the comparative model of the CARNOT toolbox (Storage Type 3, modified best-fit); b) differences between mean temperatures of CARNOT and STORE.

to the reduced volume by internal insulation components, the peak capacity level is reduced by about 11% to 23.5 MWh (Fig. 8a). The fraction of discharged thermal energy sums up to 68.8 MWh, compared to 99.1 MWh of heat charged to the basin. Due to the high insulation and reduced heat losses, the maximum storage temperature shows a 3.0 K higher value of 45.8 °C, while the average temperature of 45.2 °C is raised by about 6.1 K in comparison to the base case (Fig. 8b-c). The latter can be considered an advantage since thermal energy can be supplied at a higher exergetic level during discharge [94,95]. The significance of such exergy-based evaluations is underpinned by the results of previous studies [8] which discovered similar relationships with temperature levels and temperature stratification in the sTES facilities. However, in this case, it cannot counterbalance the reduction of capacity due to the reduced filling volume.

The operation shows effective control, especially after the charging phases. While this study does not consider a heat pump, the configured time and temperature hystereses effectively reduce periods of pump operation to promote the charging flow. Thus, as illustrated similarly in [15,29], the coefficient of performance and/or solar fraction, or renewable energy fraction of an integrated system, may be optimized. In Fig. 7a and Fig. 7e, this becomes evident by alternating operations of idle and charging. In fact, most of the idle phases in the last simulated year occur in the high-tech scenario (2,516 h), hence minimizing auxiliary energy consumption by circulating pumps, heat pumps, and other installations. In contrast, the base case scenario shows only 1,536 h of idle time periods in the last simulated year.

In the two extreme cases, as well as among all scenarios, the maximum temperature of the filling never fully reaches the temperature of the charging flow (Fig. 7b/c, Fig. 7f/g). Average temperatures range between 42.0 $^{\circ}$ C and 45.2 $^{\circ}$ C, with an offset of 2 K compared to the

maximum temperature. This is due to the heterogeneous temperature distribution in the filling. Here, the storage medium of a gravel-water mixture prevents pronounced convective thermal energy flow in comparison to the conditions in pure water TTES.

Charging and discharging are carried out indirectly from top to bottom via a pipe coil heat exchanger. As illustrated in Fig. 7c, this intensifies the characteristic internal temperature spreading and stratification within the storage in the base case scenario. However, this is mitigated by insulation as shown in Fig. 7f. Here, the more substantially homogeneous profile originates from reduced internal and external losses, which is of primary importance in exergy analyses, as similarly demonstrated in related studies [63,94]. In contrast, Fig. 7c reveals much more pronounced temperature fluctuations, predominantly in the upper storage section, which is strongly controlled by the ambient air thermal conditions.

The temperatures of the heat exchanger return flow provide information about the appropriate dimensioning of the coil system. In both scenarios, the charging/discharging flows are consistently well exploited, as the temperatures are effectively lowered to the filling temperature during charging. As depicted in Fig. 7b and Fig. 7f, the spread between supply and return flows is at its highest at the beginnings of charging and discharging periods in each year of the simulation. For charging, it is at least 45.9 K, while it reaches up to 30.1 K during discharging.

3.2.2. Effects of top covering and thermal insulation at different external interfaces

Considering minimum temperature values of the sTES filling, it becomes evident that an external top covering or insulation at the top of the basin is essential. Particularly during winter months, a risk of freezing can exist in this section of the storage, which would result in massive material degradation or even damage caused to interior components. This risk is particularly high at the beginning of storage operation, as the storage is initialized with ambient temperature. In contrast, insulation of the sidewalls and the bottom of the storage is ineffective or even adversarial, as it would prevent compensation of thermal losses by heat flux from the thermal mass of surrounding soil, which was also reported in practice [96]. The results show that at least a top covering of 1.0 m of soil is needed for ensuring a minimum temperature above 0 °C. Artificial insulation is more favorable, where a thickness of only 0.1 m already provides sufficient protection. Besides, during long-term operation, freezing may also be prevented by not fully discharging, resulting in a higher temperature at the end of the discharging period. This, however, reduces the exploitable capacity and thus the costeffectiveness of the facility.

Thermal insulation at the bottom of the storage may hinder basal heat loss, but it can also be disadvantageous. Since insulation layers were modeled as internal components, their application reduces both the volume and the capacity of the storage. While Dahash et al. [25] mention this as a theoretical issue, it is particularly striking for the results of the case study: while energy losses of lateral insulation are

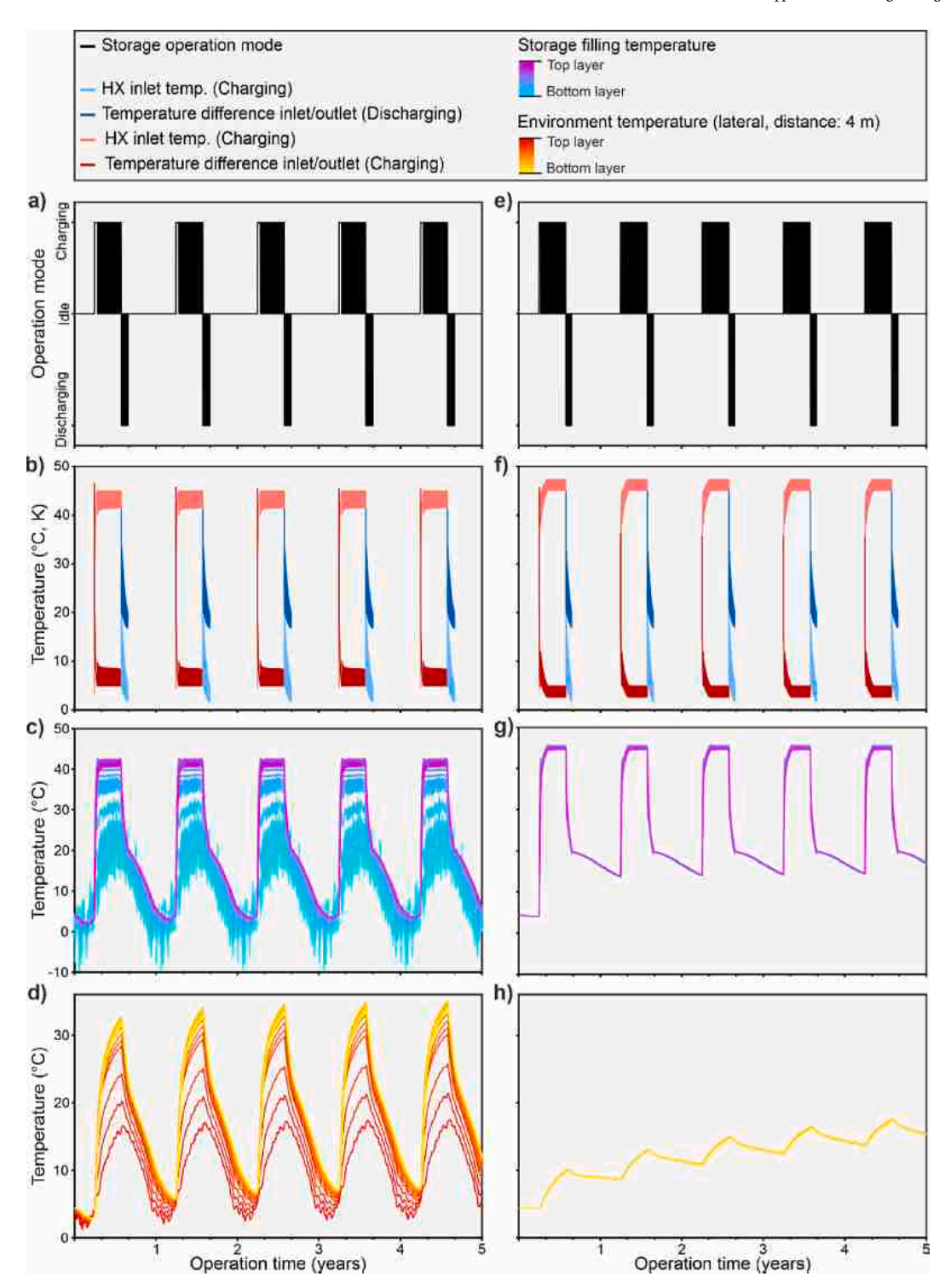


Fig. 7. Operational diagram of the base case (a-d) and the high-tech scenario (e-h). For temperatures in the heat exchanger (HX), setbacks (i.e., temperature differences to the supply) are displayed.

improved by about max. 19.2% in comparison to the base case scenario, they change negligibly if the storage is only insulated at the bottom. This is also due to the low temperatures in the lower part of the filling. Such effects are even more evident for efficiency endpoint parameters: both the storage and subsystem efficiency decrease for bottom insulations, while for wall insulations only the subsystem efficiency increases slightly (max. 15.1% for highest insulation thickness; Fig. 8d). Hence, consistent with the findings from previous studies [79,97], insulation is shown to be most efficient at the top while it is much less favorable at the

bottom.

For all scenarios, subsystem efficiencies range from 12.2% to 69.5% (Fig. 8d) and storage efficiencies from 1.4% to 57.1% (Fig. 8e). The lowest storage efficiency is found in the scenario of a 0.3 m thick sidewall insulation. In fact, an evaluation of storage quality based on this indicator alone does not appear to be suitable: in this scenario, an amount of 52.6 MWh of energy is available, while internal thermal conditions are strongly controlled by interactions with the surrounding environment. Therefore, ratings should consider both efficiency

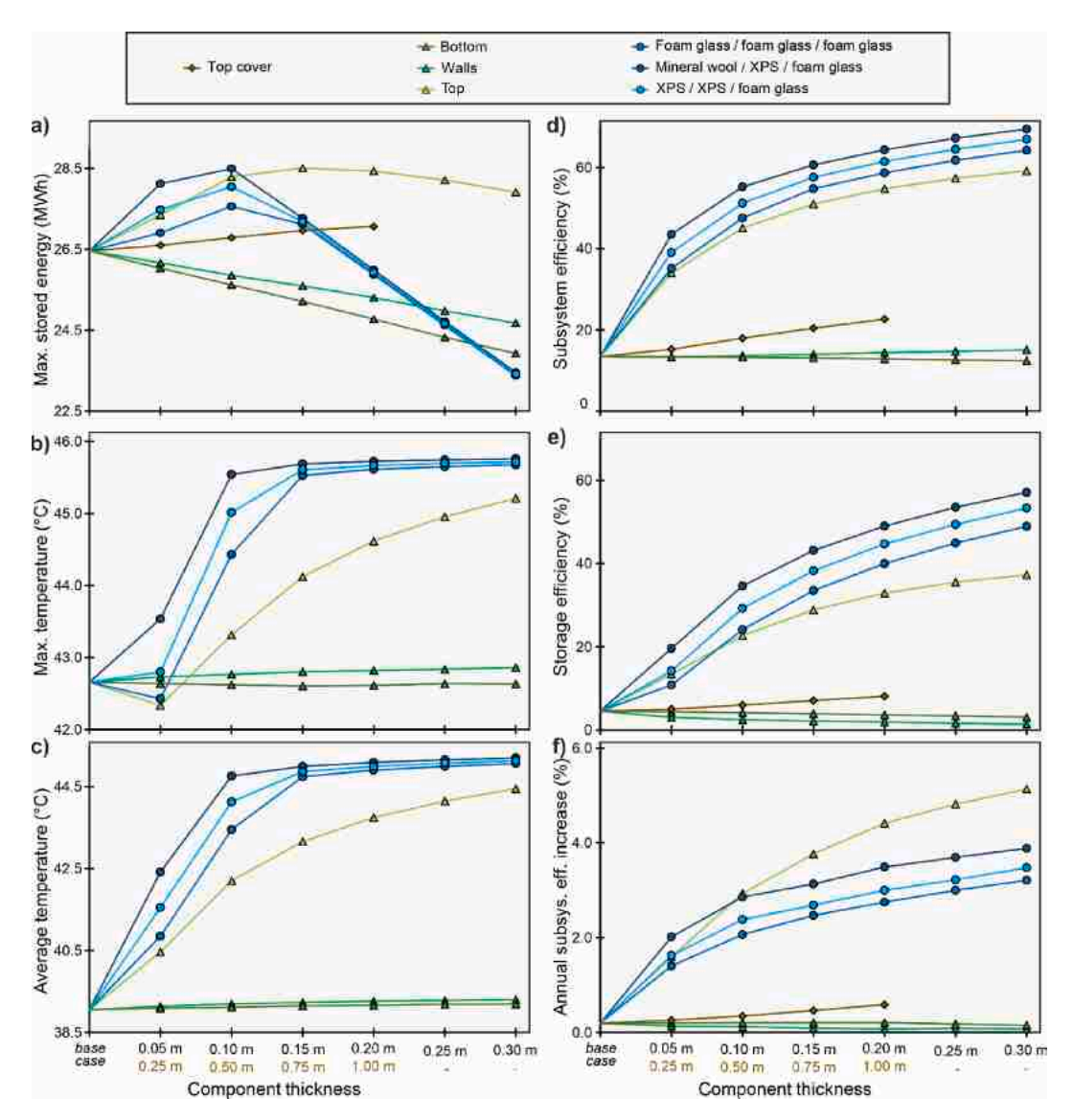


Fig. 8. Changes in evaluation parameters over the upgrade stages (increasing thicknesses) of the respective components (top covering, thermal insulations). The diagram shows a) the maximum storage level, as well as b) the maximum, and c) average filling temperatures over the entire simulation period. Furthermore, the diagram shows d-e) trends in endpoint parameters of storage and subsystem efficiency for storage upgrades, and f) annual rates of increase in the subsystem efficiency.

parameters: in that case, the high-tech scenario with 0.3 m thick, all-sided, differentiated insulation shows the best performance. With values of 57.1% and 69.5%, both storage and subsystem efficiencies are in the 90th percentile of the values of all simulated scenarios (Fig. 8d-e).

In Fig. 8a, it is furthermore demonstrated for all scenarios with internal insulation, that the maximum capacity levels of the storage unit decrease consistently with increasing insulation thickness (for sidewall and bottom insulations) or after a peak (for top and all-sided insulations). Similar results are obtained for discharge quantities, which are positively influenced by lower energy losses as the insulation increases, but negatively influenced by reduced volumes. This again supports the application of an external top cover. It achieves an efficiency increase of max. 9.2% (Fig. 8d) and does not reduce the volume capacity of the storage. It also ensures a higher maximum capacity level of 27.1 MWh (Fig. 8a).

3.2.3. Impacts of different insulation materials for all-sided insulation

The previous scenarios and analyses involved insulations on individual interfaces with only one insulation material – foam glass gravel. In further scenarios, all-sided insulations, as well as alternative

insulation materials, are inspected. Thereby, this component is replaced with XPS and/or mineral wool at the top, as well as at the sidewalls. As suggested by Marx et al. [98] and Mangold [99], this can further optimize the performance of the system by minimizing thermal losses, yet increasing the complexity and investment costs.

The results show that all-sided insulation is superior to insulation exclusively at the top from at least a thickness of 0.1 m, as insulation translates to the reduction of storage volume. Starting from the base case scenario, the improvement of the storage efficiencies is almost concurrent and not diverging with increasing insulation thickness (Fig. 8e). Based on homogeneous 0.3 m thick insulation of foam glass gravel at all sides, the storage achieves efficiency and reaches values of 48.9% (storage efficiency) and 64.2% (subsystem efficiency). In comparison to the 0.05 m thick insulation, losses are reduced significantly from 178.0 MWh to 57.7 MWh.

Enhanced material characteristics lead to a further increase in the storage efficiency by about 5% to 8%. The highest value is achieved in the high-tech scenario with 0.3 m thick insulation of mineral wool at the top, XPS at the sides, and foam glass gravel at the bottom (57.1%, Fig. 8e). Regarding average storage temperatures, no major variations

are apparent above an insulation thickness of 0.15 m; in the comparison of the maximum storage level, all three materials show similar values (Fig. 8c). This is particularly important for techno-economic optimization of storage designs. However, further factors, such as pressure stability, long-term effectiveness, and performance under the influence of groundwater or seepage penetration, must be considered [2]. Nevertheless, the installation of different materials may be associated with higher material expenses and more complicated installation methods, and should therefore be subject to a comparative cost-benefit analysis [25].

3.2.4. Long-term performance and thermal conditions in ambient subsurface

The important measures observed during the storage operation are positive and negative losses. While negative losses are directed outwards of the storage, positive losses are considered to be energy quantities absorbed from the surrounding soil. Especially for non- or low-insulated sTES systems, these may be significant or even desired. In addition, gains from solar irradiation can contribute significantly via the storage's top surface, especially in the case of black waterproofing foils and no soil cover. The results of the test study clearly show these effects, in the sense that temperatures in the topmost storage layers replicate ambient conditions in particular - both the air temperature and global irradiation profiles (Fig. 7c). This is also reflected in the temperatures of the near surrounding soil in this scenario (Fig. 7d). In comparison, temperatures of the surrounding ground in Fig. 7h no longer show strong interference of the natural ambient conditions; in contrast, they are clearly superimposed by the annual storage operation cycle, exhibiting significantly larger and phase-shifted temperature amplitudes. Multi-year simulations demonstrate this effect distinctly, as periodically heating (both laterally and below the storage) occurs even at further distances. These conclusions are supported by results gained in practice, for example from the WGTES in Stuttgart, Germany [96].

The degree to which the temperatures in the near field correlate with the average temperature of the storage depends again on the degree of insulation. Thus, heating at a distance of 2 m next to the basin is increased by a maximum of 14.1 K after five years for the high-tech scenario, but only to a maximum of 7.9 K in the case of the uninsulated base case scenario. This also compares closely to results obtained from operating installations. For example, Bodmann et al. [100] measured temperatures between 8 °C and 30 °C up to 4 m away from the TTES in Hanover, Germany, while Benner et al. [79] report a temperature increase of 9 K after one year, 2 m next to the storage in Friedrichshafen, Germany.

During long-term operation, environmental effects also lead to changes in energy flows, which ultimately result in an overall improvement of performance. As theoretically discussed by Dincer et al. [101], this mechanism is proven by the test study in all scenarios, but to different extents (Fig. 8f). While the base case shows an annual increase in the subsystem efficiency of only 0.2% over five years, this effect is most pronounced for the highest insulation at the top (0.3 m) with an increase of 5.1% per year. Although the latter scenario does not show the highest subsystem efficiency in the last simulated year, its increase from 44.3% to 67.1% reflects the initial phase of a storage's operation until peak efficiency is reached. Similar trends of heating and stabilization phases were measured for sTES systems in Steinfurt, Germany [76,100], and Hanover, Germany [100]. The efficiency increase follows a converging trend to an upper threshold for the scenarios with top and all-sided isolations. This indicates that the optimum configuration as a ratio between storage usability (by maximum discharge quantity) and capacity of the seasonal storage may already be achieved.

Excess energy quantities after the evaluation periods represent an important factor of long-term performance. In general, the highest surplus appears in the last simulated year, since increased temperatures of the surrounding soil prevent rapid and full cooling of the storage. This is most significant in the scenario of insulation exclusively with foam glass

gravel at the top, where the surplus is up to 8.34 MWh. This underlines the beneficial thermal effect of surrounding soil for ground-based systems, since energy is not lost due to effective insulation in the upper storage section, but can be recovered at the same time from the ambient ground heated up by the storage system. This effect is most potent at the beginning of the operation. With continued operation and higher temperatures of the surrounding soil, the effect changes to that of thermal activation, as losses are reduced by flattened thermal gradients.

4. Conclusions

Reliable planning of water-based seasonal thermal energy storages requires accurate and effective simulation. Several analytical and numerical solutions are at hand to model the behavior of such large-scale devices. For optimal integration, robust predictions about the operation behavior of these facilities are needed. Particularly ground-based systems with diverse geometries prove to be complex in technical respects, with regard to governing thermal processes and interference with the environment. Thus, common axially symmetric models may not be suitable for flexible geometries. Similarly, computational requirements of high-resolution computational fluid dynamics and 3D-finite element method-models are often impractical for extensive parameter studies.

To overcome these issues, the newly developed model "STORE" represents a component-based approach to combine benefits of resolving all building components and relevant processes of seasonal storages with those of comprehensive parametrization, multidimensional geometry, and versatile evaluation capabilities. Based on the Simscape library available in Matlab/Simulink, the structure and approach of STORE is first described, including processes, input and output data, and its design database for parametric studies. Accuracy and applicability are confirmed with conventional methods in a plausibility test.

The capabilities of STORE are further demonstrated in a parametric test study with 41 scenarios to identify trends of varying configurations and materials of thermal insulation. The re-use of a swimming pool (raw volume: 940 m³) with a soil top covering or different insulation thicknesses is investigated. The results reveal design recommendations for future projects:

- Thermal insulation at the top or alternatively an external top covering with soil of at least 1 m thickness is essential to guarantee fail-safe operation.
- The insulating effect is greatest when an external cover is applied, which does not reduce the storage volume and thus its capacity under similar temperature conditions. Accordingly, top insulations are most effective (since the highest temperature gradients also exist here). In contrast, bottom insulations may be adversarial by reducing the capacity, while low losses do not cause efficiency improvements.
- The use of different insulation materials at individual storage interfaces can be profitable only under certain conditions (e.g., thicknesses), underlining the benefit of simulation-based design for ascertaining optimized component configurations.
- Heating of the ambient soil results in successive performance improvements via reduced energy losses, as well as increased usability of the system with prolonged service life.
- Evaluations of different design scenarios must consider multiple criteria (e.g., maximum capacity, storage efficiency, and average temperature) to identify optimal solutions.
- These criteria may yield opposite effects (e.g., lower energy yield through reduced capacity vs. higher efficiency by increased insulation thickness). Thus, cost-benefit analyses related to improved (but costlier) insulation materials are suggested.

The results of the test study prove the flexibility and diverse evaluation capabilities of STORE. Hence, the model may be utilized in further generic studies or for case-specific planning. The opportunity for

computationally efficient, model-based technical optimization will finally enable the minimization of both capital and operational costs of seasonal thermal energy storage systems.

Declaration of Competing Interest

The authors declare that they have no known competing financial interests or personal relationships that could have appeared to influence the work reported in this paper.

Acknowledgements

The authors acknowledge Olivia Zoch and Ryan Pearson for language edits.

The present study is financially supported by the Bavarian State Ministry of Education and Culture, Science and the Arts within the framework of the "Programm zur Förderung der angewandten Forschung und Entwicklung an Hochschulen für angewandte Wissenschaften – Programmsäule Strukturimpuls – Forschungseinstieg" (grant agreement no. VIII.2-F1116.IN/19/2).

Appendix A. Supplementary data

Supplementary data to this article can be found online at https://doi.org/10.1016/j.applthermaleng.2022.118810.

References

- IEA, Market Report Series: Renewables 2019 Analysis and Forecasts to 2024, 2019.
- [2] C. Bott, I. Dressel, P. Bayer, State-of-technology review of water-based closed seasonal thermal energy storage systems, Renewable and Sustainable Energy Reviews 113 (2019), 109241.
- [3] P. Gabrielli, M. Gazzani, E. Martelli, M. Mazzotti, Optimal design of multi-energy systems with seasonal storage, Applied Energy 219 (2018) 408–424.
- [4] S. Kalaiselvam, R. Parameshwaran, Thermal Energy Storage Technologies for Sustainability: Systems Design, Elsevier, Assessment and Applications, 2014.
- [5] J. Xu, R.Z. Wang, Y. Li, A review of available technologies for seasonal thermal energy storage, Solar Energy 103 (2014) 610–638.
- [6] C.N. Antoniadis, G. Martinopoulos, Simulation of Solar Thermal Systems with Seasonal Storage Operation for Residential Scale Applications, Procedia Environmental Sciences 38 (2017) 405–412.
- [7] I. Beausoleil-Morrison, B. Kemery, A.D. Wills, C. Meister, Design and simulated performance of a solar-thermal system employing seasonal storage for providing the majority of space heating and domestic hot water heating needs to a singlefamily house in a cold climate, Solar Energy 191 (2019) 57–69.
- [8] M. Jonin, M. Khosravi, A. Eichler, W. Villasmil, P. Schuetz, C.N. Jones, R. S. Smith, Exergy-based model predictive control for design and control of a seasonal thermal energy storage system, J. Phys.: Conf. Ser. 1343 (2019) 12066.
- [9] M.L. Sweet, J.T. McLeskey, Numerical simulation of underground Seasonal Solar Thermal Energy Storage (SSTES) for a single family dwelling using TRNSYS, Solar Energy 86 (2012) 289–300.
- [10] A. Ucar, M. Inalli, A thermo-economical optimization of a domestic solar heating plant with seasonal storage, Applied Thermal Engineering 27 (2007) 450–456.
- [11] M. Chung, J.-U. Park, H.-K. Yoon, Simulation of a central solar heating system with seasonal storage in korea, Solar Energy 64 (1998) 163–178.
- [12] J.D. Hunt, B. Zakeri, W. Leal Filho, P.S. Schneider, N.d.A.B. Weber, L.W. Vieira, C. Ermel, N.J. de Castro, P.S.F. Barbosa, A. Nascimento, A. Mastrucci, Swimming pool thermal energy storage, an alternative for distributed cooling energy storage, Energy Conversion and Management 230 (2021) 113796.
- [13] V. Tulus, D. Boer, L.F. Cabeza, L. Jiménez, G. Guillén-Gosálbez, Enhanced thermal energy supply via central solar heating plants with seasonal storage: A multiobjective optimization approach, Applied Energy 181 (2016) 549–561.
- [14] T. Urbaneck, J.M. Mücke, F. Findeisen, M. Gensbaur, S. Lang, D. Bestenlehner, H. Drück, R. Beyer, K. Pieper, Demonstration of an Overground Hot Water Store in Segmental Construction for District Heating Systems, Energy Procedia 149 (2018) 615–624.
- [15] J. Zhao, L. Lyu, X. Li, Numerical analysis of the operation regulation in a solar heating system with seasonal water pool thermal storage, Renewable Energy 150 (2020) 1118–1126.
- [16] P. Bayer, G. Attard, P. Blum, K. Menberg, The geothermal potential of cities, Renewable and Sustainable Energy Reviews 106 (2019) 17–30.
- [17] P. Fleuchaus, B. Godschalk, I. Stober, P. Blum, Worldwide application of aquifer thermal energy storage—A review, Renewable and Sustainable Energy Reviews 94 (2018) 861–876.

- [18] P. Bayer, M. de Paly, M. Beck, Strategic optimization of borehole heat exchanger field for seasonal geothermal heating and cooling, Applied Energy 136 (2014) 445–453.
- [19] D. Rohde, T. Andresen, N. Nord, Analysis of an integrated heating and cooling system for a building complex with focus on long-term thermal storage, Applied Thermal Engineering 145 (2018) 791–803.
- [20] E. Saloux, J.A. Candanedo, Optimal rule-based control for the management of thermal energy storage in a Canadian solar district heating system, Solar Energy 207 (2020) 1191–1201.
- [21] L. Xu, J.I. Torrens, F. Guo, X. Yang, J.L. Hensen, Application of large underground seasonal thermal energy storage in district heating system: A model-based energy performance assessment of a pilot system in Chifeng, China, Applied Thermal Engineering 137 (2018) 319–328.
- [22] D. Panno, A. Buscemi, M. Beccali, C. Chiaruzzi, G. Cipriani, G. Ciulla, V. Di Dio, V. Lo Brano, M. Bonomolo, A solar assisted seasonal borehole thermal energy system for a non-residential building in the Mediterranean area, Solar Energy 192 (2019) 120–132.
- [23] C.R. Matos, J.F. Carneiro, P.P. Silva, Overview of Large-Scale Underground Energy Storage Technologies for Integration of Renewable Energies and Criteria for Reservoir Identification, Journal of Energy Storage 21 (2019) 241–258.
- [24] A. Hesaraki, S. Holmberg, F. Haghighat, Seasonal thermal energy storage with heat pumps and low temperatures in building projects—A comparative review, Renewable and Sustainable Energy Reviews 43 (2015) 1199–1213.
- [25] A. Dahash, F. Ochs, M.B. Janetti, W. Streicher, Advances in seasonal thermal energy storage for solar district heating applications: A critical review on largescale hot-water tank and pit thermal energy storage systems, Applied Energy 239 (2019) 296–315.
- [26] C. Chang, Z. Wu, H. Navarro, C. Li, G. Leng, X. Li, M. Yang, Z. Wang, Y. Ding, Comparative study of the transient natural convection in an underground water pit thermal storage, Applied Energy 208 (2017) 1162–1173.
- [27] Y. Bai, M. Yang, J. Fan, X. Li, L. Chen, G. Yuan, Z. Wang, Influence of geometry on the thermal performance of water pit seasonal heat storages for solar district heating, Build, Simul, 2020.
- [28] T. Schmidt, T. Pauschinger, P.A. Sørensen, A. Snijders, R. Djebbar, R. Boulter, J. Thornton, Design Aspects for Large-scale Pit and Aquifer Thermal Energy Storage for District Heating and Cooling, Energy Procedia 149 (2018) 585–594.
- [29] X. Li, Z. Wang, J. Li, M. Yang, G. Yuan, Y. Bai, L. Chen, T. Xu, A. Gilmanova, Comparison of control strategies for a solar heating system with underground pit seasonal storage in the non-heating season, Journal of Energy Storage 26 (2019), 100963.
- [30] A. Rosato, A. Ciervo, G. Ciampi, M. Scorpio, S. Sibilio, Impact of seasonal thermal energy storage design on the dynamic performance of a solar heating system serving a small-scale Italian district composed of residential and school buildings, Journal of Energy Storage 25 (2019), 100889.
- [31] J. Allegrini, K. Orehounig, G. Mavromatidis, F. Ruesch, V. Dorer, R. Evins, A review of modelling approaches and tools for the simulation of district-scale energy systems, Renewable and Sustainable Energy Reviews 52 (2015) 1391–1404
- [32] H. Cheng, J. Wu, Z. Luo, F. Zhou, X. Liu, T. Lu, Optimal Planning of Multi-Energy System Considering Thermal Storage Capacity of Heating Network and Heat Load, IEEE Access 7 (2019) 13364–13372.
- [33] J. Yuan, C. Cui, Z. Xiao, C. Zhang, W. Gang, Performance analysis of thermal energy storage in distributed energy system under different load profiles, Energy Conversion and Management 208 (2020), 112596.
- [34] A. Castell, M. Medrano, C. Solé, L.F. Cabeza, Dimensionless numbers used to characterize stratification in water tanks for discharging at low flow rates, Renewable Energy 35 (2010) 2192–2199.
- [35] J. Fernández-Seara, F.J. Uhía, J. Sieres, Experimental analysis of a domestic electric hot water storage tank. Part II: dynamic mode of operation, Applied Thermal Engineering 27 (2007) 137–144.
- [36] R. Egging-Bratseth, H. Kauko, B.R. Knudsen, S.A. Bakke, A. Ettayebi, I.R. Haufe, Seasonal storage and demand side management in district heating systems with demand uncertainty, Applied Energy 285 (2021), 116392.
- [37] R. McKenna, D. Fehrenbach, E. Merkel, The role of seasonal thermal energy storage in increasing renewable heating shares: A techno-economic analysis for a typical residential district, Energy and Buildings 187 (2019) 38–49.
- [38] K. Narula, F. de Oliveira Filho, J. Chambers, E. Romano, P. Hollmuller, M. K. Patel, Assessment of techno-economic feasibility of centralised seasonal thermal energy storage for decarbonising the Swiss residential heating sector, Renewable Energy 161 (2020) 1209–1225.
- [39] C. Suárez, J. Pino, F. Rosa, J. Guerra, Analytical approach to ground heat losses for high temperature thermal storage systems, Int J Energy Res 43 (2019) 439–454.
- [40] E. Hahne, Y. Chen, Numerical study of flow and heat transfer characteristics in hot water stores, Solar Energy 64 (1998) 9–18.
- [41] F. Ochs, A. Dahash, A. Tosatto, M. Bianchi Janetti, Techno-economic planning and construction of cost-effective large-scale hot water thermal energy storage for Renewable District heating systems, Renewable Energy 150 (2020) 1165–1177.
- [42] Tosatto, A., Dahash, A., Ochs, F., Bianchi Janetti, M., Development of a Numerical Model for Large-Scale Seasonal Thermal Energy Storage for District Heating Systems, in: COMSOL Conference 2019, Cambridge, 2019.
- [43] F. Ochs, A. Dahash, A. Tosatto, M. Reisenbichler, K. O'Donovan, G. Gauthier, C.K. Skov, T. Schmidt, Comprehensive Comparison of Different Models for Large-Scale Thermal Energy Storage, in: Proceedings of the International Renewable Energy Storage Conference 2021 (IRES 2021), Atlantis PressParis, France, 2022, pp. 36–51.

- [44] U.-M. Solar Energy Laboratory, TRNSYS: A TRaNsient SYstems Simulation Program. Version 18.0, Solar Energy Laboratory, UW-Madison, Wisconsin-Madison, USA., 2021.
- [45] L.T. Terziotti, M.L. Sweet, J.T. McLeskey, Modeling seasonal solar thermal energy storage in a large urban residential building using TRNSYS 16, Energy and Buildings 45 (2012) 28–31.
- [46] M. Wetter, W. Zuo, T.S. Nouidui, X. Pang, Modelica Buildings library, Journal of Building Performance Simulation 7 (2014) 253–270.
- [47] M. Wetter, M. Bonvini, T.S. Nouidui, W. Zuo, Modelica buildings library 2.0, in: Proc, Simulation Association, Hyderabad, India, 2015.
- [48] Introduction to COMSOL multiphysics®, 1998.
- [49] ANSYS Inc., Ansys Fluent: Fluid Simulation Software, 2021, https://www.ansys.com/de-de/products/fluids/ansys-fluent, accessed 11 March 2022.
- [50] H.-J.G. Diersch, FEFLOW: Finite Element Modeling of Flow, Mass and Heat Transport in Porous and Fractured Media, Springer Science & Business Media, 2013
- [51] A. Dahash, F. Ochs, A. Tosatto, W. Streicher, Toward efficient numerical modeling and analysis of large-scale thermal energy storage for renewable district heating, Applied Energy 279 (2020), 115840.
- [52] L. Amiri, S.A. Ghoreishi-Madiseh, A.P. Sasmito, F.P. Hassani, A porous medium based heat transfer and fluid flow model for thermal energy storage in packed rock beds, IOP Conf. Ser.: Earth Environ. Sci. 268 (2019) 12100.
- [53] J. Fan, J. Huang, A. Chatzidiakos, S. Furbo, Experimental and theoretic investigations of thermal behavior of a seasonal water pit heat storage, Solar World Congress, in, 2017.
- [54] D. Sun, J. Xu, P. Ding, Performance Analysis and Application of Three Different Computational Methods for Solar Heating System with Seasonal Water Tank Heat Storage, Advances in Mechanical Engineering 5 (2013), 857941.
- [55] K.M. Powell, T.F. Edgar, An adaptive-grid model for dynamic simulation of thermocline thermal energy storage systems, Energy Conversion and Management 76 (2013) 865–873.
- [56] A. Dahash, F. Ochs, A. Tosatto, Co-Simulation of Dynamic Energy System Simulation and COMSOL Multiphysics, in: COMSOL Conference 2019, Cambridge, 2019.
- [57] H. Bastida, C.E. Ugalde-Loo, M. Abeysekera, M. Qadrdan, J. Wu, N. Jenkins, Dynamic Modelling and Control of Thermal Energy Storage, Energy Procedia 158 (2019) 2890–2895.
- [58] F. Ochs, Large-Scale Thermal Energy Stores in District Heating Systems Simulation Based Optimization, in, International Solar Energy Society, Freiburg, Germany, 2015.
- [59] M.V. Jensen, J.E. Nielsen, Seasonal pit heat storages Guidelines for materials & construction: IEA SHC FACT SHEET 55.C-D2, 2020.
- [60] G. Gauthier, Benchmarking, and improving models of subsurface heat storage dynamics. Comparison of Danish PTES and BTES installation measurements with their corresponding TRNSYS models, GEOTHERMICA – ERA NET Cofund Geothermal (2020).
- [61] L. Mazzarella, Multi-flow stratified thermal storage model with full-mixed layers: Type 142, Institut für Thermodynamik und Wärmetechnik Universität Stuttgart-FRG, Stuttgart, 1992.
- [62] M. Homberger, "ICEPIT"—A TRNSYS model for cold storage., in: Proceedings of EUROTHERM Seminar, Physical Models for Thermal Energy Stores No. 49 (1996).
- [63] Y. Bai, Z. Wang, J. Fan, M. Yang, X. Li, L. Chen, G. Yuan, J. Yang, Numerical and experimental study of an underground water pit for seasonal heat storage, Renewable Energy 150 (2020) 487–508.
- [64] K. Narula, F.D.O. Filho, J. Chambers, M.K. Patel, Simulation and comparative assessment of heating systems with tank thermal energy storage – A Swiss case study, Journal of Energy Storage 32 (2020), 101810.
- [65] K. Narula, F. de Oliveira Filho, W. Villasmil, M.K. Patel, Simulation method for assessing hourly energy flows in district heating system with seasonal thermal energy storage, Renewable Energy 151 (2020) 1250–1268.
- [66] P. Sorknæs, Simulation method for a pit seasonal thermal energy storage system with a heat pump in a district heating system, Energy 152 (2018) 533–538.
- [67] A. Dahash, F. Ochs, A. Tosatto, Simulation-based design optimization of largescale seasonal thermal energy storage in renewables-based district heating systems. in: Proceedings of BauSIM 2020 Conference, 2020.
- [68] M. Reisenbichler, K. O'Donovan, C.R. Tugores, W.V. Helden, F. Wotawa, Towards More Efficient Modeling and Simulation of Large-Scale Thermal Energy Storages in Future Local and District Energy Systems, in: Proceedings of Building Simulation 2021, 2021.
- [70] C. Wemhöner, B. Hafner, K. Schwarzer, Simulation of solar thermal systems with CARNOT blockset in the environment Matlab/Simulink, in: Eurosun 2000, Copenhagen, 2000.
- [71] A. Dahash, M.B. Janetti, F. Ochs, Detailed 3-D models of a large-scale underground thermal energy storage with consideration of groundwater conditions, in: International Sustainable Energy Conference 2018, Graz, Austria, 2018, pp. 597–604.
- [72] F. Ochs, Modelling Large-Scale Thermal Energy Stores. Dissertation, Stuttgart, 2009.
- [73] MathWorks, R2021a at a Glance, 2021, https://www.mathworks.com/products/ new_products/latest_features.html, accessed 7 September 2021.

- [74] MathWorks, Simscape Model and simulate multidomain physical systems (Version 5.0), 2021, https://www.mathworks.com/help/physmod/simscape/, accessed 7 September 2021.
- [75] T. Urbaneck, U. Schirmer, Central solar heating plant with gravel water storage in Chemnitz (Germany), in: M. Benner, E. Hahne (Eds.), Terrastock 2000: Terrastock 2000, 8th International 8th Conference on Thermal Energy Storage, 1st ed., Stuttgart. 2000.
- [76] M. Bodmann, H. Koch, M.N. Fisch, Solare Nahwärmeversorgung mit Kies/ Wasserspeicher in Steinfurt-Borghorst, in, OPET-Seminar Solarunterstützte Nahwärmeversorgung (2001).
- [77] A. Saggion, R. Faraldo, M. Pierno, Thermodynamics, Springer International Publishing, Cham, 2019.
- [78] T. Urbaneck, Berechnung von Kies-Wasser-Speichern. Dissertation, Chemnitz, 2004.
- [79] M. Benner, M. Bodmann, D. Mangold, J. Nußbicker, S. Raab, T. Schmidt, H. Seiwald, Solar unterstützte Nahwärmeversorgung mit und ohne Langzeit-Wärmespeicher: Forschungsbericht zum BMBF/BMWA-Vorhaben (November 1998 bis Januar 2003), Stuttgart, 2003.
- [80] V. Gnielinski, Neue Gleichungen für den Wärme-und den Stoffübergang in turbulent durchströmten Rohren und Kanälen, Forschung im Ingenieurwesen 41 (1975) 8–16.
- [81] V. Gnielinski, New equations for heat and mass transfer in turbulent pipe and channel flow, Int. Chem. Eng. 16 (1976) 359–368.
- [82] Verein Deutscher Ingenieure, VDI-Gesellschaft Verfahrenstechnik und Chemieingenieurwesen (GVC), VDI-Wärmeatlas: Berechnungsblätter für den Wärmeübergang, Springer, Berlin Heidelberg, Berlin, Heidelberg, s.l., 2002.
- [83] CARNOT. Solar-Institut Juelich, V. Toolbox, for Matlab/Simulink R2018b. User Manual 7 (2020) 07/2019. https://de.mathworks.com/matlabcentral/fileexchange/68890-carnot-toolbox.
- [84] R. Ilgaz, R. Yumrutaş, Heating performance of swimming pool incorporated solar assisted heat pump and underground thermal energy storage tank: A case study, Int J Energy Res (2021).
- [85] G. Emmi, A. Natali, S. Cesari, P. Fausti, M. Bottarelli, Use of an Outdoor Swimming Pool as Seasonal Heat Source in Heat Pump Applications, TI-IJES 65 (2021) 337–344.
- [86] T. Urbaneck, B. Platzer, U. Schirmer, Advanced Monitoring of gravel water storage, in. Futurestock 2003: 9th International Conference on Thermal Energy Storage, 2003.
- [87] F. Ochs, W. Heidemann, H. Müller-Steinhagen, H. Koch, Soil-Water Pit Heat Store with direct charging system: Technology and Economy, in: S. Burek, M.G. Hutchins, H. Lockhart Ball, S. Abrahamson (Eds.), EuroSun 2006, 2006.
- [88] Ecoglas, Technische Daten, 2021, https://www.ecoglas.de/files/Technische-Daten.pdf, accessed 10 June 2021.
- [89] G. Oliveti, N. Arcuri, Prototype Experimental Plant for the Interseasonal Storage of Solar Energy for the Winter Heating of Buildings: Description of Plant and its Functions, Solar Energy 54 (1995) 85–97.
- [90] Deutsches Institut für Normung e.V. (DIN), Wärmeschutz und Energie-Einsparung in Gebäuden - Teil 4: Wärme- und feuchteschutztechnische Bemessungswerte (Thermal insulation and energy economy in buildings - Part 4: Hygrothermal design values), Beuth, Berlin, 2020, https://www.beuth.de/de/norm/din-4108-4/327502903, accessed 10 September 2021.
- [91] Guadalfjara, M., Lozano, M. A., Serra, L. M., Analysis of Large Thermal Energy Storage for Solar District Heating, in: Eurotherm Seminar #99.
- [92] BBSR, Ortsgenaue Testreferenzjahre (TRY) von Deutschland für mittlere und extreme Witterungsverhältnisse: Release date: 2021-06-08. Test datasets for environmental conditions, Deutscher Wetterdienst (German Weather Service), Bonn, 2017.
- [93] W.R. van WIJK, Physics of Plant Environment, Soil Science 98 (1964) 69.
- [94] A. Dahash, F. Ochs, A. Tosatto, Techno-economic and exergy analysis of tank and pit thermal energy storage for renewables district heating systems, Renewable Energy 180 (2021) 1358–1379.
- [95] M.A. Rosen, I. Dincer, Exergy methods for assessing and comparing thermal storage systems, International Journal of Energy Research 27 (2003) 415–430.
- [96] E. Hahne, The ITW solar heating system: an oldtimer fully in action, Solar Energy 69 (2000) 469–493.
- [97] A. Matthees, P. Stange, A. Hülser, K. Rühling, GREEN HEAT³: Entwicklung innovativer Energieversorgungstechniken und -strukturen mit den Kernkomponenten modularer Großwärmespeicher und Maxianlage Solarthermie, in: Symposium Solarthermie - Technik für die Energiewende, 2018, pp. 389–401.
- [98] R. Marx, J. Nußbicker-Lux, D. Bauer, W. Heidemann, H. Drück, Saisonale Wärmespeicher - Bauarten, Betriebsweise und Anwendungen, Chemie Ingenieur Technik 83 (2011) 1994–2001.
- [99] D. Mangold, Erfahrungen und Ergebnisse aus der Umsetzung der Budnesforschungsprogramme Solarthermie-2000 und Solarthermie2000plus: Input zu EU-Vorhaben Solarge (Solarthermische Großanlagen), Target GmbH, Hannover, 2006.
- [100] M. Bodmann, M.N. Fisch, Solar unterstützte Nahwärmeversorgung: Pilotprojekte Hamburg, Hannover und Steinfurt, in: 5. FKS-Symposium: FKS-Forschungskreis Solarenergie, 2004.
- [101] İ. Dinçer, M. Rosen, Thermal energy storage: Systems and applications, 2nd ed., Wiley, Hoboken N.J., 2011.